Since January 2020 Elsevier has created a COVID-19 resource centre with free information in English and Mandarin on the novel coronavirus COVID-19. The COVID-19 resource centre is hosted on Elsevier Connect, the company's public news and information website.

Current Research in Chemical Biology 2 (2022) 100025

Contents lists available at ScienceDirect

Current Research in Chemical Biology

journal homepage: www.journals.elsevier.com/current-research-in-chemical-biology

Repurposing Halicin as a potent covalent inhibitor for the SARS-CoV-2 main protease

Kai S. Yang [a,1], Syuan-Ting Alex Kuo [a,1], Lauren R. Blankenship [a], Zhi Zachary Geng [a], Shuhua G. Li [a], David H. Russell [a], Xin Yan [a], Shiqing Xu [a,*], Wenshe Ray Liu [a,b,c,d,**]

[a] Texas A&M Drug Discovery Laboratory, Department of Chemistry, Texas A&M University, College Station, TX, 77843, USA
[b] Department of Biochemistry and Biophysics, Texas A&M University, College Station, TX, 77843, USA
[c] Institute of Biosciences and Technology and Department of Translational Medical Sciences, College of Medicine, Texas A&M University, Houston, TX, 77030, USA
[d] Department of Molecular and Cellular Medicine, College of Medicine, Texas A&M University, College Station, TX, 77843, USA

A B S T R A C T

The rapid spread of COVID-19 has caused a worldwide public health crisis. For prompt and effective development of antivirals for SARS-CoV-2, the pathogen of COVID-19, drug repurposing has been broadly conducted by targeting the main protease (M^{Pro}), a key enzyme responsible for the replication of virus inside the host. In this study, we evaluate the inhibition potency of a nitrothiazole-containing drug, halicin, and reveal its reaction and interaction mechanism with M^{Pro}. The *in vitro* potency test shows that halicin inhibits the activity of M^{Pro} an IC_{50} of 181.7 nM. Native mass spectrometry and X-ray crystallography studies clearly indicate that the nitrothiazole fragment of halicin covalently binds to the catalytic cysteine C145 of M^{Pro}. Interaction and conformational changes inside the active site of M^{Pro} suggest a favorable nucleophilic aromatic substitution reaction mechanism between M^{Pro} C145 and halicin, explaining the high inhibition potency of halicin towards M^{Pro}.

1. Introduction

The ongoing pandemic of coronavirus disease 2019 (COVID-19) has led to catastrophic impacts on the whole world. Its scale and duration have surpassed the 1918 influenza pandemic (Gates, 2020; Morens et al., 2020). As of Feb 1st, 2022, the total number of confirmed global COVID-19 cases is about 376 million, of which 5.6 million have succumbed to death (WHO data) (WHO, 2022). The current available vaccines and drugs against COVID-19 have led to lots of exciting innovations (Torgovnick, 2021; An EUA for sotrovimab for, 2021; Drozdzal et al., 2021; Li et al., 2022). However, new SARS-CoV-2 variants that display attenuated responses or complete evasion of vaccine protection and developed drug resistant strains have been continuously emerging (Vilar and Isom, 2021). In the context of the disastrous damage of COVID-19 to public health, civil society and the global economy, the search for effective drugs against new strains of SARS-CoV-2 is still in urgent demand.

Given the rapid spread and high fatality of COVID-19, drug repurposing stands out as an attractive and quick access to effective antivirals. If an approved drug could be identified to treat COVID-19, it can promptly proceed to clinical trials and GMP manufacture. Previously, encouraging results that show antiviral activity against SARS-CoV-2 were obtained from repurposing small molecule medicines including remdesivir, ritonavir/lopinavir, bepridil and nitazoxanide (Chakraborty et al., 2021; Vatansever et al., 2021; Morse et al., 2020). Nitazoxanide was developed as an antiparasitic agent especially against *Cryptosporidium* spp. A later *in vitro* assessment of nitazoxanide has confirmed its promising activity against SARS-CoV-2 with an EC_{50} value as 2.12 μM (Stachulski et al., 2021). Several clinical trials that are evaluating the use of nitazoxanide for the treatment of COVID-19 are currently underway or in development. Nitazoxanide is a nitrothiazole-containing compound (Fig. 1A). Another notable compound that belongs to the same group is halicin (Fig. 1A). Halicin (formerly known as SU3327) is an inhibitor of the enzyme c-Jun N-terminal kinase (JNK) which regulates important cellular activities including cell proliferation, differentiation, and apoptosis. It was first predicted by molecular modeling that halicin binds at the active site of JNK with its nitrothiazole group and blocks the access of JNK to its substrates. Further mice studies also showed the ability of halicin to significantly reduce blood glucose levels and restore insulin sensitivity in a type-2 diabetes mouse model (De et al., 2009). More recently, driven by a deep neural network assisted drug

* Corresponding author.
** Corresponding author. Texas A&M Drug Discovery Laboratory, Department of Chemistry, Texas A&M University, College Station, TX, 77843, USA.
E-mail addresses: shiqing.xu@tamu.edu (S. Xu), wsliu2007@tamu.edu (W.R. Liu).
[1] Contributed equally to the paper.

https://doi.org/10.1016/j.crchbi.2022.100025
Received 28 February 2022; Received in revised form 30 March 2022; Accepted 7 April 2022

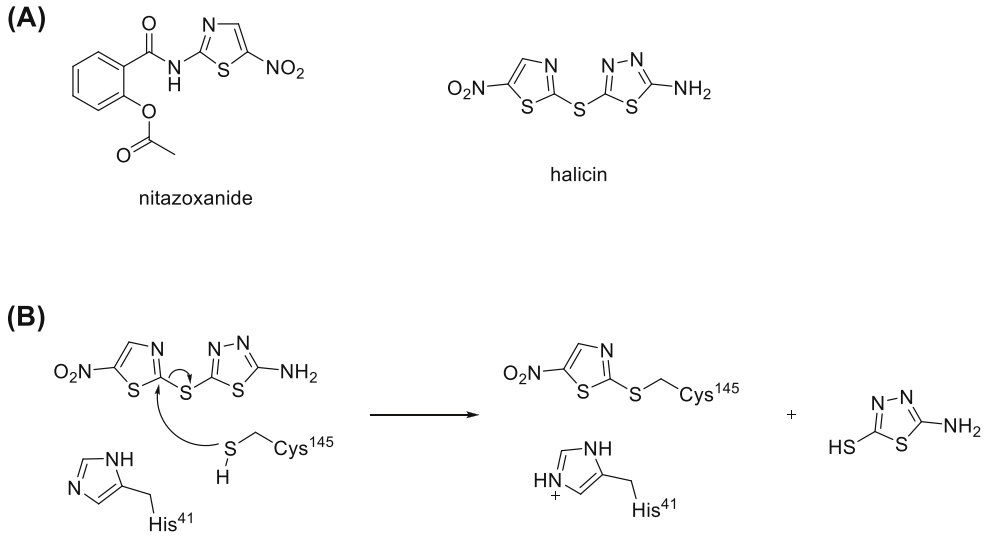

Fig. 1. (A) Structure of nitazoxanide and halicin. (B) Proposed reaction mechanism between halicin and cysteine.

prediction, halicin was discovered to play a role against a wide phylogenetic spectrum of pathogens. This research suggested that halicin associates to the bacterial membrane by binding to the iron ion, and dissipates the ΔpH component of the proton motive force (Stokes et al., 2020). However, its capability to inhibit SARS-CoV-2 has not been studied yet.

In order to assess the antiviral activity of halicin against SARS-CoV-2, a specific target from SARS-CoV-2 needs to be chosen. A quick molecular docking of halicin against main protease (M^{Pro}), one of the promising drug targets of SARS-CoV-2, shows that halicin could well fit into the active site of M^{Pro} with a reasonable binding energy as −6.1 kcal/mol (Fig. S1). This interesting result encourage us to further explore the inhibition of halicin on M^{Pro}. M^{Pro} has been widely targeted to conduct drug repurposing for SARS-CoV-2 because of its essential role in virus replication and pathogenesis (Vatansever et al., 2021). It is a peptide fragment of pp1a and pp1ab, two translation products from the SARS-CoV-2 RNA genome after the virus infects human cells (V'Kovski et al., 2021). Both pp1a and pp1ab are very large polypeptides that need to undergo proteolytic hydrolysis to form a number of nonstructural proteins (Nsps) which are essential for the virus to replicate its genome in host cells, evade from the host immune system, and package new virions for infection of new host cells (V'Kovski et al., 2021). M^{Pro} processes 13 out of the total 16 Nsps. The crystal structure of M^{Pro} was resolved recently (Zhang et al., 2020). The structure shows M^{Pro} comprising of three domains, among which the first two have an antiparallel β-barrel structure, and the third has five α-helices that form an antiparallel conglomerate and connect to the first two domains by a long loop region. In its active site it has a C145–H41 catalytic dyad with the substrate-binding site located between domains (Banerjee et al., 2021). M^{Pro} exits as a homodimer in solution, and the dimer form is highly active compared to the monomer form (Grum-Tokars et al., 2008). Therefore, small-molecule medicines that specifically target SARS-CoV-2 M^{Pro} should be potentially effective treatment options for COVID-19 (Yang et al., 2021).

Inspired by the above ideas and also taking advantage of previous drug repurposing efforts on M^{Pro} of SARS-CoV-2 in our lab (Vatansever et al., 2021), we herein aim to assess the potency of halicin against M^{Pro} of SARS-CoV-2 and identify the inhibition mechanism between them. In this article, *in vitro* potency analysis was conducted and shows that halicin has a potent IC_{50} value of 0.182 μM against M^{Pro}. Mass spectrometry analysis indicated that only the nitrothiazole part of halicin covalently binds to M^{Pro}. These results were further supported by the resolution of the crystal structure of the M^{Pro}-halicin complex. The current study encourages further exploration of halicin-like molecules as COVID-19 therapeutics.

2. Results and discussion

2.1. IC_{50} determination of halicin against M^{Pro}

The potency assessment of halicin on M^{Pro} started by testing its IC_{50} *in vitro* and using nitazoxanide as a comparison. First, the compounds were incubated with 50 nM M^{Pro} at 37 °C for 30 min. Then the reaction was initiated by adding 100 μM of Sub3, a fluorescent substrate of M^{Pro} (Vatansever et al., 2021). The assay was monitored by a plate reader with Ex336/Em455 for 30 min. The first 10 min was fitted with linear regression by GraphPad Prism. The initial slope value was used as normalized activity. As shown in Fig. 2, halicin has a determined IC_{50} value as 181.7 nM, while nitazoxanide with the concentration up to 200 μM did not show any inhibition of M^{Pro} activity. This IC_{50} value of halicin is lower than most of the noncovalent inhibitors of M^{Pro} (Vatansever et al., 2021). Considering the relatively large active pocket size of M^{Pro}, halicin is not supposed to be big enough to fully occupy the active site to achieve this level of potency as a noncovalent inhibitor. Based on the above assumption, halicin was proposed to be a covalent inhibitor for M^{Pro}.

2.2. Mass spectral identification of covalent binding between M^{Pro} and halicin

In order to verify the covalent binding assumption for halicin, a sample of M^{Pro} incubated with halicin was subjected to native mass spectrometry analysis. Interestingly, binding between M^{Pro} and halicin was observed as shown in the native mass spectra (Fig. 3). The M^{Pro}-halicin complex was identified on the basis of the measured and calculated mass shifts. Notably, Fig. 3A shows that both the monomer and the dimer of the main protease can bind to halicin. The binding patterns were distinct from a reported inhibitor, GC376, which only binds to the dimeric form of M^{Pro} (Fu et al., 2020), suggesting the N-finger may not be essential for halicin to bind with the main protease. A mass shift of 127 Da was identified in the monomeric region (Fig. 3B), corresponding to only half of halicin with 1 Da deviation (Table 1, Fig. S2). In the dimeric region, the M^{Pro} was found to bind to two half halicin fragments, resulting in a 256 Da mass shift (Fig. 3C). These results indicate that

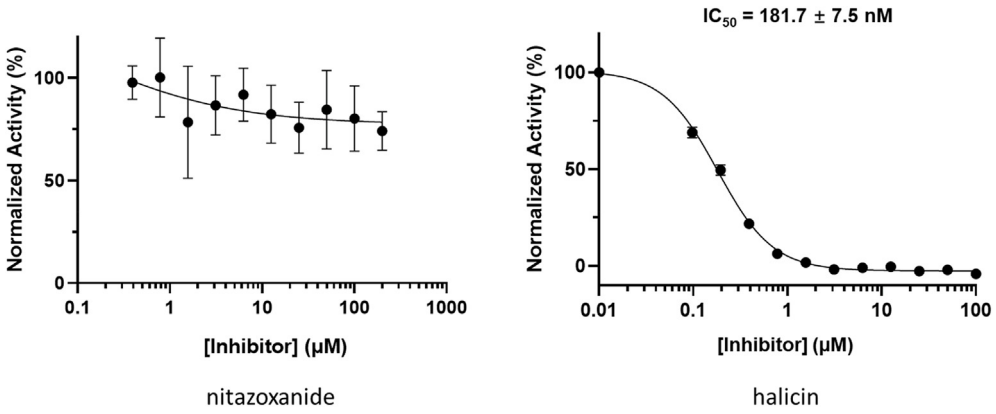

Fig. 2. IC_{50} test of nitazoxanide and halicin against M^{Pro}. Triplicate experiments were performed for each compound. GraphPad Prism 8.0 was used to perform data analysis.

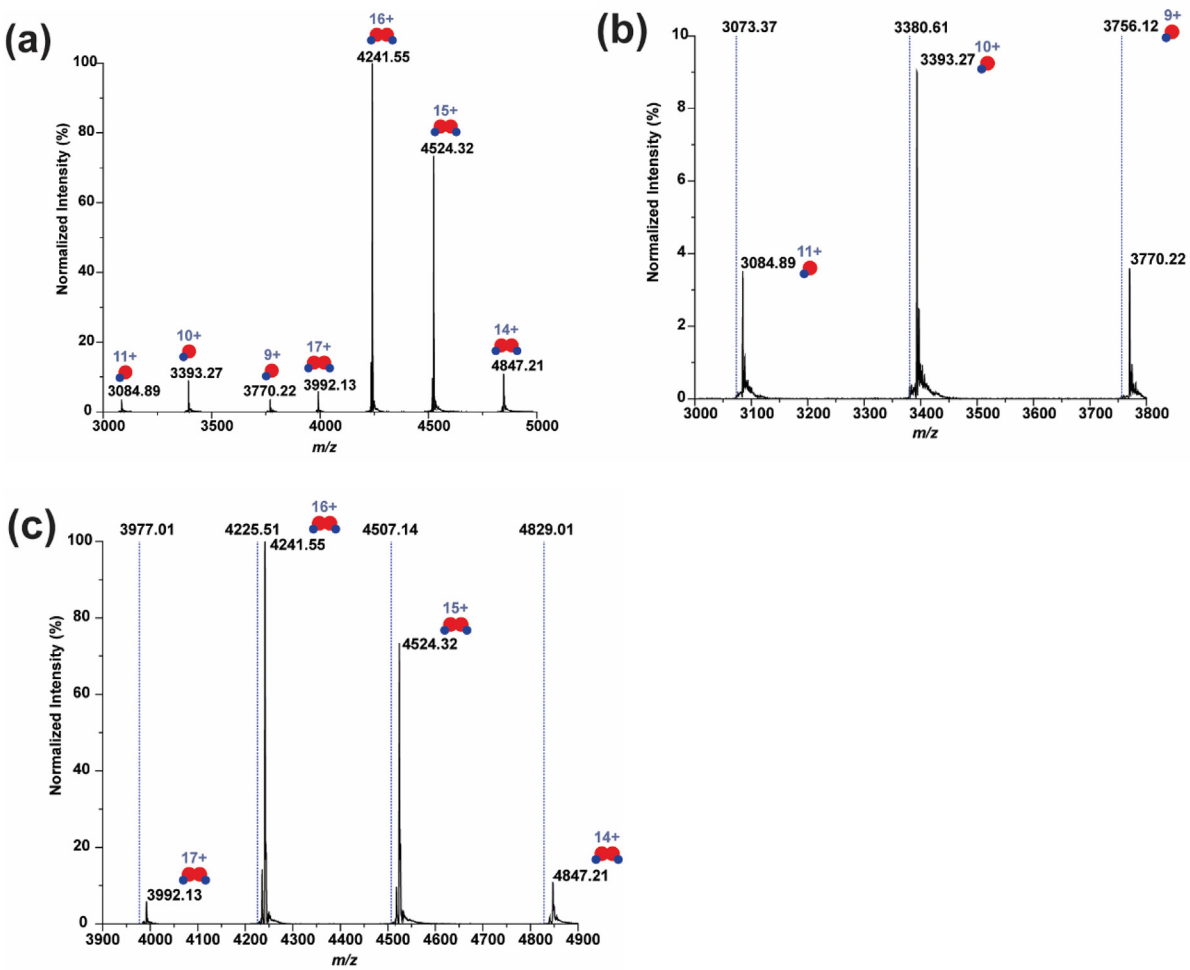

Fig. 3. Identification of halicin bound M^{Pro} by native mass spectrometry. (a) The whole spectrum (m/z from 3000 to 5000) of 2 μM main protease with 10 μM halicin. (b) The zoomed spectrum of the monomer region (m/z from 3000 to 3800). (c) The zoomed spectrum of the dimer region (m/z from 3900 to 4900). The dash lines in (b) and (c) indicate the expected m/z of the unbound main protease based on the protein sequence (Molecular weight = 33,796 Da).

halicin can bind to M^{Pro} in both catalytically inert monomeric and active dimeric forms via a mode of action of covalent binding.

2.3. *X-ray crystallography analysis of M^{Pro} bound with halicin*

To further characterize the interactions between M^{Pro} and halicin, we crystallized M^{Pro} in its apo form, soaked apo-M^{Pro} crystals with halicin, and then determined structures of M^{Pro} bound with halicin using X-ray crystallography. The complex structure was determined to a resolution of 1.85 Å with an R/R_{free} value of 24.9/27.2 (Table S2). *2Fo-Fc* electron density map around C145, C156 and C300 clearly indicates a ligand fragment covalently bound to these three cysteines respectively (Fig. 4A). Ligand building inside the *2Fo-Fc* electron density map shows that the nitrothiazole fragment of halicin fits perfectly. This is consistent with the

Table 1
Native mass spectrometry analysis of halicin-bound M^{Pro}.

	Unbound protein	Bound protein	Calculated Ligand Molecular Weight	Theoretical Ligand Molecular Weight
Monomer	33,796	33,923	127	128
Dimer	67,592	67,848	128 (Gates, 2020)	

(Gates, 2020) A dimer can bind two inhibitors. The calculated ligand molecular weight. $= \frac{MW_{bound} - MW_{unbound}}{2}$

mass spectrometry analysis that showed the addition of 127 Da to the monomeric M^{Pro}. In the M^{Pro}-halicin crystal structure, three nitrothiazole fragments rather than one were observed on an M^{Pro} monomer. A possible reason for this result is the high concentration of halicin that was used to soak apo-M^{Pro} crystals and the exposure of C156 and C300 of M^{Pro}. Since the active site C145 is the most active one and the only one responsible for the activity of M^{Pro} (Zhang et al., 2020), only interactions around C145 will be further discussed.

From the surface binding model (Fig. 4B), we observed a nitrothiazole fragment of halicin forms a covalent bond with C145 and fits into the area between P1 and P2 sub-pockets. The shortest distance from the thiazole ring of nitrothiazole to the imidazole ring of H41 was measured as 3.4 Å (Fig. 4C). This indicated a van der Waals interaction between nitrothiazole and the side chain of H41. Interestingly, a comparison between structure of nitrothiazole-bound M^{Pro} and apo-M^{Pro} indicates that the side chain of H41 flips 90° to allow nitrothiazole to fit into the binding pocket, and the van der Waals interaction further stabilizes the binding of nitrothiazole to M^{Pro} (Fig. S3). Structure superposition of nitrothiazole-bound M^{Pro} and apo-M^{Pro} also shows an unfolding of α-helix in the P2 sub-pocket, which could be another adaptation of the active site pocket to the binding of nitrothiazole (Fig. S3).

The native mass spectrometry analysis that detected halicin-bound M^{Pro} and X-ray crystallography analysis of the M^{Pro}-halicin complex provide solid evidence to support the mode of action of covalent binding. A possible mechanism is shown in Fig. 1B. Halicin forms a covalent adduct with the catalytic cysteine, Cys145, via nucleophilic aromatic substitution (S_NAr) of 5-nitrothiazole and 5-amino-1,3,4-thiadiazole-2-thiol serves as a leaving group with the assistance of the catalytic base His41. Since 5-amino-1,3,4-thiadiazole fragment falls off after halicin reacts with Cys145 of M^{Pro}, we do not have structural insights about how 5-amino-1,3,4-thiadiazole contributes to the binding before the formation of a covalent adduct. Considering the favorable binding of 5-nitrothiazole to the M^{Pro} active site and high reactivity of halicin with cysteine, our study provides a potential tunable S_NAr-based reactive group of 5-nitrothiazole for selectively targeting the catalytic cysteine Cys145 of M^{Pro} by tuning 5-amino-1,3,4-thiadiazole moiety of halicin.

3. Conclusion

Researchers have predicted that additional coronavirus diseases may emerge with higher frequencies. For both combating the current pandemic and preparing to contain future coronavirus disease outbreaks, it is imperative to discover antivirals that can be applied generally to inhibit coronaviruses, and drug repurposing turns out to be an efficient way to achieve. Due to its conserveness among coronaviruses, M^{Pro} is an attractive drug target for broad-spectrum antivirals. Inspired by recent drug repurposing efforts on SARS-CoV-2 with nitazoxanide, we identified another nitrothiazole-containing drug, halicin, to successfully inhibit the activity of M^{Pro} *in vitro*. Our mass spectrometry analysis indicated that halicin binds covalently to M^{Pro} with a nitrothiazole fragment at a 1:1 ratio. A determined X-ray crystal structure of the M^{Pro}-halicin complex further confirmed the covalent binding of nitrothiazole fragment to C145 in the active site of M^{Pro}. Our results revealed high inhibition potency of halicin on M^{Pro} and uncovered its underlying S_NAr-based binding mechanism. As far as we know, this is the first S_NAr-based covalent inhibitor for M^{Pro}, indicating that a large variety of mechanistically similar compounds may be tested as M^{Pro} inhibitors to search for anti-SARS-CoV-2 therapeutics. Although the cellular experiment showed no inhibition of halicin against M^{Pro} that was transiently expressed in 293T cells (Fig. S4), this could because by the stability and permeability issues related to halicin in cells. Structure-activity relationship studies based on halicin to pursue higher potency and overcome stability and permeability concerns are worth exploring in the future for the development of drugs as SARS-CoV-2 antivirals.

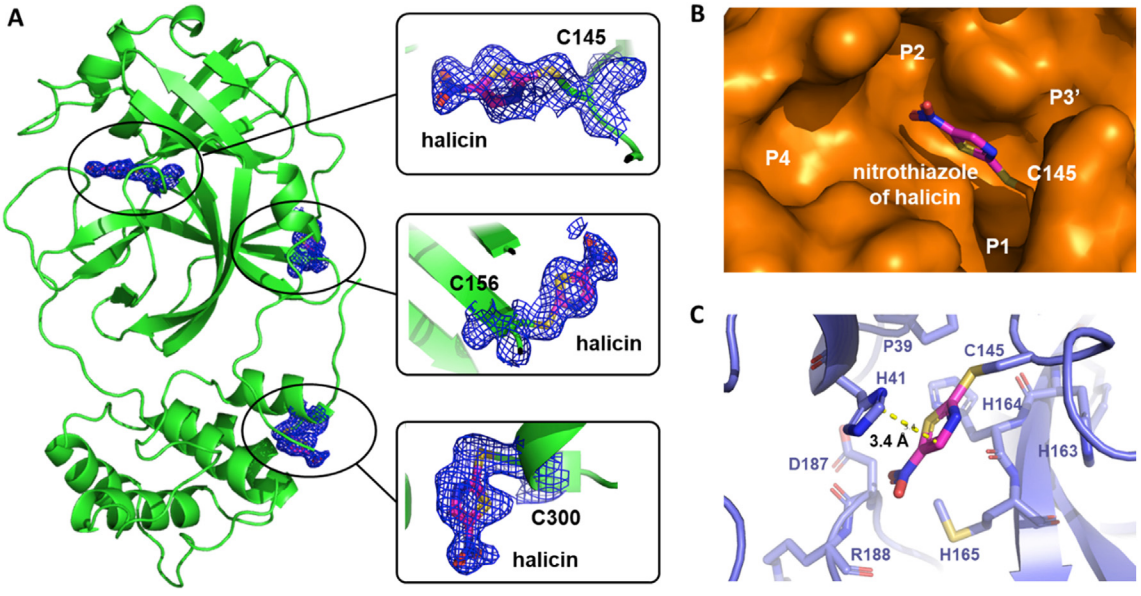

Fig. 4. Crystal structure of M^{Pro} bound with halicin (PDB ID 7TUU). (A) Location of bound halicin on M^{Pro}. Halicin was observed to bind with C145, C156 and C300. (B) Surface of M^{Pro} active site was shown. Halicin forms covalent bond with C145 and embeds between P1 and P2 sub-pockets. (C) Interaction between halicin and active site residues in M^{Pro} was shown. The shortest distance from the thiazole ring of halicin to the imidazole ring of H41 was measured as 3.4 Å and indicated as a yellow dotted line.

4. Materials and methods

4.1. Chemical

Halicin was purchased from Millipore Sigma (CAS No. 40045-50-9).

4.2. Recombinant M^{Pro} protein expression and purification

The pET28a-His-SUMO-M^{Pro} construct was made based on a pET28a plasmid modified with an N-terminal His-SUMO tag. The gene encoding M^{Pro} was amplified from a previous plasmid pBAD-sfGFP-M^{Pro} using the forward primer 5′-CGCGGATCCGGGTTTCGCAAG-3′ and the reverse primer 5′- CCGCTCGAGTTACTGAAAAGTTACGCC-3′. The amplified PCR product was digested by *BamHI* and *XhoI* and ligated into the vector pET28a-His-SUMO plasmid that was digested with the same restriction enzymes. The gene sequence of His-SUMO-M^{Pro} was verified by sequencing at Eton Bioscience Inc.

The pET28a-His-SUMO-M^{Pro} construct was transformed into *E. coli* BL21(DE3) cells. Transformed cells were cultured at 37 °C in 6 L 2xYT medium with kanamycin (50 g/mL) for 3 h and induced with isopropyl-D-1-thiogalactoside (IPTG) at final concentration of 1 mM when the OD_{600} reached 0.8. After 3 h, cells were harvested by centrifugation at 12,000 rpm, 4 °C for 30 min. Cell pellets were resuspended in 150 mL buffer A (20 mM Tris, 100 mM NaCl, 10 mM imidazole, pH 8.0) and then lysed by sonication on ice. The lysate was clarified by centrifugation at 16,000 rpm, 4 °C for 30 min. The supernatant was loaded onto a nickel-chelating column with high affinity Ni-charged resin from GenScript and washed with 10 column volumes of buffer A to remove nonspecifically bound proteins, which was followed by elution using buffer B (20 mM Tris, 100 mM NaCl, 250 mM imidazole, pH 8.0). The protein eluates were subjected to buffer exchange with buffer C (20 mM Tris, 10 mM NaCl, 1 mM dithiothreitol (DTT), pH 8.0) by using a HiPrep 26/10 desalting column (GE Healthcare). The His-SUMO-M^{Pro} proteins were digested with SUMO protease overnight at 4 °C. The digested protein was applied to a nickel-chelating column again to remove the His-tagged SUMO protease, the His-SUMO tag, and the expressed protein with uncleaved His-SUMO tag. The tag-free M^{Pro} protein was loaded onto an anion-exchange column with Q Sepharose, Fast Flow (GE Healthcare) equilibrated with buffer C for further purification. The column was eluted by buffer D (20 mM Tris, 1 M NaCl, 1 mM DTT, pH 8.0) with a linear gradient ranging from 0 to 500 mM NaCl. Fractions eluted from the anion exchange column were condensed and loaded to a size exclusion column with HiPrep 16/60 Sephacryl S-100 HR (GE Healthcare) pre-equilibrated with buffer E (20 mM Tris, 100 mM NaCl, 1 mM DTT, 1 mM EDTA, pH 7.8). The eluted M^{Pro} protein in buffer E was concentrated to 20 mg/mL and stored in −80 °C for further use.

4.3. IC_{50} analysis

The assays were carried out with 50 nM enzyme and 10 μM substrate at 37 °C with continuous shaking. The Sub3 substrate (DABCYL-Lys-Thr-Ser-Ala-Val-Leu-Gln-Ser-Gly-Phe-Arg-Lys-Met-Glu-EDANS) was purchased from BACHEM and stored as 1 mM solution in 100% DMSO. Enzyme activity was monitored by detecting fluorescence with excitation at 336 nm and emission at 455 nm wavelength. The dilution buffer (used for enzyme and substrate dilution) is 10 mM $Na_xH_yPO_4$,10 mM NaCl, 0.5 mM EDTA, pH 7.6. Final composition of the assay buffer is 10 mM $Na_xH_yPO_4$, 10 mM NaCl, 0.5 mM EDTA, 2 μM DTT (coming from enzyme stock solution), pH 7.6 with 1.25% DMSO. Inhibitors were stored as 10 mM in 100% DMSO solutions in a −20 °C freezer.

For the IC_{50} analysis, the inhibitor was diluted to 400-fold times higher than the highest working concentration to make the secondary stock solution (i.e. if the highest working concentration of inhibitor is 2 μM, then the inhibitor was diluted from its 10 mM stock solution to 800 μM in DMSO). 10 μL from this secondary stock solution was added to 990 μL of the dilution buffer. Serial dilutions were carried out in the dilution buffer containing 1% DMSO to ensure all the inhibitor serial dilutions contained 1% DMSO. 25 μL of each inhibitor solution were added to a 96-well plate with a multichannel pipettor. Next, 25 μL of a 200 nM enzyme solution (diluted from 10 μM enzyme storage solution in 10 mM $Na_xH_yPO_4$,10 mM NaCl, 0.5 mM EDTA, pH 7.6, 1 mM DTT in the dilution buffer) was added by a multichannel pipettor and mixed by pipetting up and down three times. Then, the enzyme-inhibitor solution was incubated at 37 °C for 30 min. During the incubation period, 20 μM of the substrate solution was prepared by diluting from 1 mM stock solution in the dilution buffer. When the incubation period was over, 50 μL of the 20 μM substrate solution was added to each well using a multichannel pipettor and the assay started. Data recording was stopped after 30 min. Data treatment was done with GraphPad Prism 8.0. The first 0–300 s were analyzed by linear regression for initial slope analyses. Then, the initial slopes were normalized and IC_{50} values were determined by inhibitor vs response - Variable slope (four parameters).

4.4. Mass spectrum analysis

The main protease was desalted into a 200 mM ammonium acetate using a Bio-Spin column (BIO-RAD) with 6k cut-off. After desalting, the main protease was mixed with halicin. The final concentration of protein and halicin was 2 μM and 10 μM, respectively. The protein/halicin solution was incubated for 15 min at room temperature prior to mass spectrometry analysis. Native mass spectrometry (nMS) analysis was performed on a ThermoFisher Q-Exactive Plus UHMR with spray voltage set to 1.0–1.3 kV. Desolvation and removal of non-specific adducts were performed using a capillary temperature of 120 °C, the in-source trapping energy of −10 V, and the HCD cell collision energies of 30 V.

4.5. X-ray crystallography analysis of M^{Pro}-Inhibitor complexes

The production of crystals of halicin bound M^{Pro} complexes was following the previous protocols (Yang et al., 2021). The data was collected on a Bruker Photon II detector. The diffraction data were indexed, integrated and scaled with PROTEUM3. All the structures were determined by molecular replacement using the structure model of the free enzyme of the SARS-CoV-2 M^{Pro} [Protein Data Bank (PDB) ID code 7JPY] as the search model using Phaser in the Phenix package (Yang et al., 2021; Winn et al., 2011). *JLigand* and *Sketcher* from the CCP4 suite were employed for the generation of PDB and geometric restraints for the inhibitors. The inhibitors were built into the *Fo-Fc* density by using *Coot* (Emsley et al., 2010). Refinement of the structure was performed with Real-space Refinement in Phenix (Adams et al., 2010). Details of data quality and structure refinement are summarized in Table S2. All structural figures were generated with PyMOL (https://www.pymol.org).

4.6. The cellular inhibition potency characterization of halicin

We followed a previously established procedure strictly to characterize the cellular inhibition potency of halicin (Cao et al., 2022). Cells transfected with the pLVX-M^{Pro}-eGFP-2 plasmid were cultured together with different concentrations of halicin as 10, 2, 0.4, 0.08, 0.016, 0.0032 or 0 μM and analyzed by flow cytometry. MPI8 was used as a positive control. (Yang et al., 2021; Ma et al., 2022).

4.7. The docking parameters and methods

In addition to receptor and ligand preparations, AutoDockTools-1.5.7 was also used for grid parameter setting. The cognate ligand of crystal structure 7JQ5 of M^{Pro} suggested the inhibitor binding site. A grid box with dimensions 30 × 30 × 30 centered at the coordinates X = −10.0, Y = 13.0, and Z = 70.0 was used to represent the search space. An AutoDock Vina docking protocol was used with options of 20 CPUs and maximum 100 binding modes for undergoing calculation. Only modes with the highest binding affinities were analyzed.

Declaration of competing interest

The authors declare that they have no known competing financial interests or personal relationships that could have appeared to influence the work reported in this paper.

Acknowledgments

This work was supported in part by the Welch Foundation grants A-1715 and A-2089, the Texas A&M X-Grants mechanism and the U.S. National Institutes of Health grants R35GM143047, P41GM128577 and R01GM138863.

Appendix A. Supplementary data

Supplementary data to this article can be found online at https://doi.org/10.1016/j.crchbi.2022.100025.

References

Adams, P.D., Afonine, P.V., Bunkoczi, G., Chen, V.B., Davis, I.W., Echols, N., Headd, J.J., Hung, L.W., Kapral, G.J., Grosse-Kunstleve, R.W., et al., 2010. PHENIX: a comprehensive Python-based system for macromolecular structure solution. Acta. Crystallogr D Biol. Crystallogr. 66, 213–221.

An EUA for sotrovimab for treatment of COVID-19. Med. Lett. Drugs Ther. 63, 2021, 97–xx98.

Banerjee, R., Perera, L., Tillekeratne, L.M.V., 2021. Potential SARS-CoV-2 main protease inhibitors. Drug Discov. Today 26, 804–816.

Cao, W., Cho, C.D., Geng, Z.Z., Shaabani, N., Ma, X.R., Vatansever, E.C., Alugubelli, Y.R., Ma, Y., Chaki, S.P., Ellenburg, W.H., et al., 2022. Evaluation of SARS-CoV-2 main protease inhibitors using a novel cell-based assay. ACS Cent. Sci. 8, 192–204.

Chakraborty, C., Sharma, A.R., Bhattacharya, M., Agoramoorthy, G., Lee, S.S., 2021. The drug repurposing for COVID-19 clinical trials provide very effective therapeutic combinations: lessons learned from major clinical studies. Front. Pharmacol. 12, 704205.

De, S.K., Stebbins, J.L., Chen, L.H., Riel-Mehan, M., Machleidt, T., Dahl, R., Yuan, H., Emdadi, A., Barile, E., Chen, V., et al., 2009. Design, synthesis, and structure-activity relationship of substrate competitive, selective, and in vivo active triazole and thiadiazole inhibitors of the c-Jun N-terminal kinase. J. Med. Chem. 52, 1943–1952.

Drozdzal, S., Rosik, J., Lechowicz, K., Machaj, F., Szostak, B., Przybycinski, J., Lorzadeh, S., Kotfis, K., Ghavami, S., Los, M.J., 2021. An update on drugs with therapeutic potential for SARS-CoV-2 (COVID-19) treatment. Drug Resist. Updates 59, 100794.

Emsley, P., Lohkamp, B., Scott, W.G., Cowtan, K., 2010. Features and development of Coot. Acta. Crystallogr D Biol. Crystallogr. 66, 486–501.

Fu, L., Ye, F., Feng, Y., Yu, F., Wang, Q., Wu, Y., Zhao, C., Sun, H., Huang, B., Niu, P., et al., 2020. Both Boceprevir and GC376 efficaciously inhibit SARS-CoV-2 by targeting its main protease. Nat. Commun. 11, 4417.

Gates, B., 2020. Responding to Covid-19 - a once-in-a-century pandemic? N. Engl. J. Med. 382, 1677–1679.

Grum-Tokars, V., Ratia, K., Begaye, A., Baker, S.C., Mesecar, A.D., 2008. Evaluating the 3C-like protease activity of SARS-Coronavirus: recommendations for standardized assays for drug discovery. Virus Res. 133, 63–73.

Li, D., Sempowski, G.D., Saunders, K.O., Acharya, P., Haynes, B.F., 2022. SARS-CoV-2 neutralizing antibodies for COVID-19 prevention and treatment. Annu. Rev. Med. 73, 1–16.

Ma, X.R., Alugubelli, Y.R., Ma, Y., Vatansever, E.C., Scott, D.A., Qiao, Y., Yu, G., Xu, S., Liu, W.R., 2022. MPI8 is potent against SARS-CoV-2 by inhibiting dually and selectively the SARS-CoV-2 main protease and the host Cathepsin L. ChemMedChem 17, e202100456.

Morens, D.M., Daszak, P., Taubenberger, J.K., 2020. Escaping pandora's box - another novel coronavirus. N. Engl. J. Med. 382, 1293–1295.

Morse, J.S., Lalonde, T., Xu, S., Liu, W.R., 2020. Learning from the past: possible urgent prevention and treatment options for severe acute respiratory infections caused by 2019-nCoV. Chembiochem 21, 730–738.

Stachulski, A.V., Taujanskas, J., Pate, S.L., Rajoli, R.K.R., Aljayyoussi, G., Pennington, S.H., Ward, S.A., Hong, W.D., Biagini, G.A., Owen, A., et al., 2021. Therapeutic potential of nitazoxanide: an appropriate choice for repurposing versus SARS-CoV-2? ACS Infect. Dis. 7, 1317–1331.

Stokes, J.M., Yang, K., Swanson, K., Jin, W., Cubillos-Ruiz, A., Donghia, N.M., MacNair, C.R., French, S., Carfrae, L.A., Bloom-Ackermann, Z., et al., 2020. A deep learning approach to antibiotic discovery. Cell 180, 688–702 e613.

Torgovnick, J., 2021. Effectiveness of Covid-19 vaccines against the B.1.617.2 (delta) variant. N. Engl. J. Med. 385, e92.

V'Kovski, P., Kratzel, A., Steiner, S., Stalder, H., Thiel, V., 2021. Coronavirus biology and replication: implications for SARS-CoV-2. Nat. Rev. Microbiol. 19, 155–170.

Vatansever, E.C., Yang, K.S., Drelich, A.K., Kratch, K.C., Cho, C.C., Kempaiah, K.R., Hsu, J.C., Mellott, D.M., Xu, S., Tseng, C.K., et al., 2021. Bepridil is potent against SARS-CoV-2 in vitro. Proc. Natl. Acad. Sci. U. S. A. 118, e2012201118.

Vilar, S., Isom, D.G., 2021. One year of SARS-CoV-2: how much has the virus changed? Biology 10, 91.

WHO, 2022. WHO Coronavirus (COVID-19) Dashboard.

Winn, M.D., Ballard, C.C., Cowtan, K.D., Dodson, E.J., Emsley, P., Evans, P.R., Keegan, R.M., Krissinel, E.B., Leslie, A.G., McCoy, A., et al., 2011. Overview of the CCP4 suite and current developments. Acta. Crystallogr D Biol. Crystallogr. 67, 235–242.

Yang, K.S., Ma, X.R., Ma, Y., Alugubelli, Y.R., Scott, D.A., Vatansever, E.C., Drelich, A.K., Sankaran, B., Geng, Z.Z., Blankenship, L.R., et al., 2021. A quick route to multiple highly potent SARS-CoV-2 main protease inhibitors*. ChemMedChem 16, 942–948.

Zhang, L., Lin, D., Sun, X., Curth, U., Drosten, C., Sauerhering, L., Becker, S., Rox, K., Hilgenfeld, R., 2020. Crystal structure of SARS-CoV-2 main protease provides a basis for design of improved alpha-ketoamide inhibitors. Science 368, 409–412.